AD-A115 390 NAVAL SURFACE WEAPONS CENTER DAHLGREN VA F/G 17/7
SIMULTANEOUS OBSERVATIONS OF GLOBAL POSITIONING SYSTEM (GPS) SA--ETC(U)
MAR 82 B R HERMANN, A G EVANS
UNCLASSIFIED NSWC/TR-81-472 NL

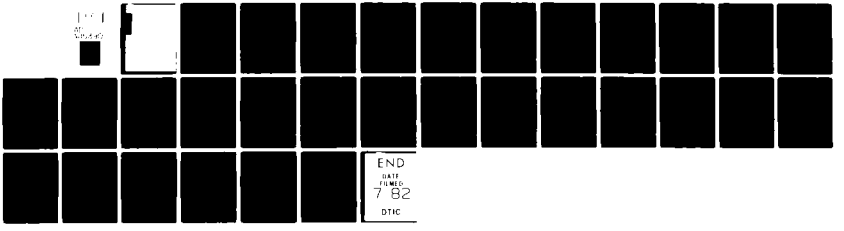

END
DATE FILMED
7 82
DTIC

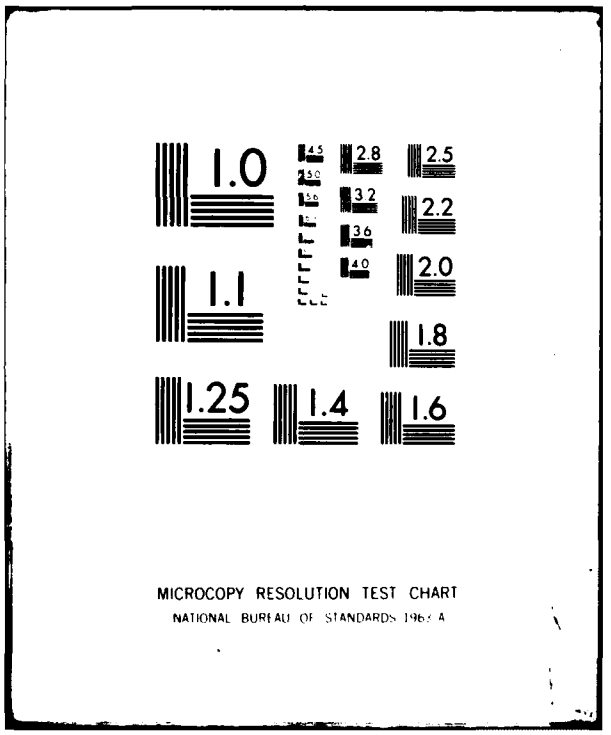
1.0
1.1
1.25
1.4
1.6
1.8
2.0
2.2
2.5
2.8
3.2
3.6
4.0
MICROCOPY RESOLUTION TEST CHART
NATIONAL BUREAU OF STANDARDS 1963 A

UNCLASSIFIED

SECURITY CLASSIFICATION OF THIS PAGE (When Data Entered)

REPORT DOCUMENTATION PAGE		READ INSTRUCTIONS BEFORE COMPLETING FORM
1. REPORT NUMBER NSWC TR 81-472	2. GOVT ACCESSION NO. AD-A115390	3. RECIPIENT'S CATALOG NUMBER
4. TITLE (and Subtitle) SIMULTANEOUS OBSERVATIONS OF GLOBAL POSITIONING SYSTEM (GPS) SATELLITES WITH TWO NAVSTAR GEODETIC RECEIVER SYSTEMS (NGRSs)		5. TYPE OF REPORT & PERIOD COVERED Final 6. PERFORMING ORG. REPORT NUMBER
7. AUTHOR(s) Bruce R. Hermann Alan G. Evans		8. CONTRACT OR GRANT NUMBER(s)
9. PERFORMING ORGANIZATION NAME AND ADDRESS Naval Surface Weapons Laboratory (K13) Dahlgren, VA 22448		10. PROGRAM ELEMENT, PROJECT, TASK AREA & WORK UNIT NUMBERS 63701B
11. CONTROLLING OFFICE NAME AND ADDRESS Defense Mapping Agency Hydrographic/Topographic Center Washington, DC 20315		12. REPORT DATE March 1982 13. NUMBER OF PAGES 34
14. MONITORING AGENCY NAME & ADDRESS(if different from Controlling Office)		15. SECURITY CLASS. (of this report) UNCLASSIFIED 15a. DECLASSIFICATION/DOWNGRADING SCHEDULE

16. DISTRIBUTION STATEMENT (of this Report)

Approved for public release; distribution unlimited.

17. DISTRIBUTION STATEMENT (of the abstract entered in Block 20, if different from Report)

18. SUPPLEMENTARY NOTES

19. KEY WORDS (Continue on reverse side if necessary and identify by block number)

NAVSTAR Geodetic Receiver System (NGRS)
Global Positioning System (GPS)
Pseudorange Measurement
Range Difference Observations
Analog Doppler Signals

20. ABSTRACT (Continue on reverse side if necessary and identify by block number)

Two conventional code tracking Global Positioning System (GPS) receiver systems were used to simultaneously track GPS satellites on a short baseline. Six-second pseudorange observations and range differences from 1-min Doppler counts at a single frequency were obtained from each receiver. Relative positioning of the receiver antennas was conducted over zero-length and 2-m baselines. Common and independent frequency standards were used on different days; the results were compared.

DD FORM 1 JAN 73 1473 EDITION OF 1 NOV 65 IS OBSOLETE
S/N 0102-LF-014-6601

UNCLASSIFIED

SECURITY CLASSIFICATION OF THIS PAGE (When Data Entered)

FOREWORD

The development of the NAVSTAR Geodetic Receiver System (NGRS) was funded by the Defense Mapping Agency as a means to demonstrate the capability of using the Global Positioning System (GPS) transmissions to achieve high-accuracy geodetic positioning. The receiver was designed by Stanford Telecommunications Incorporated. The supporting hardware and the system microprocessor controller software were proposed and implemented at the Naval Surface Weapons Center (NSWC) by the Advanced Projects Division, Electronics Systems Department. Data reduction was performed by the Space Flight Sciences Branch and the Physical Sciences Software Branch of the Space and Surface Systems Division, Strategic Systems Department. Technical and administrative assistance was received from the sponsor through the Defense Mapping Agency Hydrographic/Topographic Center, Washington, D.C.

Released by:

C. A. FISHER, Head
Strategic Systems Department

CONTENTS

	Page
INTRODUCTION	1
NGRS DATA DESCRIPTION	2
FORMULATION	2
OBSERVATIONS	7
NOISE PROBLEM	8
SOLUTIONS	17
DAYS 10 AND 12	17
DAYS 15 AND 16	19
DAYS 17, 18, AND 19	19
CONCLUSIONS	24
REFERENCES	24
DISTRIBUTION	

INTRODUCTION

NSWC has developed two Navstar Geodetic Receiver Systems (NGRSs) that utilize Stanford Telecommunication Inc. (STI) GPS receivers. The first NGRS was operational in February 1979, and data was gathered at several sites in the United States during that year. Throughout 1980, the first system was progressively modified so that it and the second system (developed in 1980) had as much common hardware and software as practical. The primary differences between the two systems are related to the differences in the two STI receivers employed: the first NGRS utilizes a STI model 5007 receiver, while NGRS-2 utilizes a model 5010. The later model 5010 has the capability of L_2 pseudorange observations and also provides dual-frequency 6-s digital Doppler count output, while the 5007 does not.

Each system, which is composed of the components listed in Table 1, is mounted in three 5-ft racks. The microprocessor software and the processing software that reads the recorded data tapes were developed at NSWC. A more detailed system description is given in Reference 1.

Table 1. NGRS Components

Microprocessor Controller	INTEL 80/10
Frequency Standard	HP 5061A-004
GPS Receiver	STI 5007 or STI 5010
GPS Test Transmitter	STI 5001A
Time-Interval Counters	HP 5370 and HP 5328
Full-Cycle Doppler Counter	NSWC
Digital Clock	HP 59309A
Antenna	CKU CA3207
Tape Recorder	KENNEDY 9800
Keyboard/Display	ADM-3
Power Buffer	ELGAR UPS 252-1

NGRS DATA DESCRIPTION

The original intent of the NGRS was to utilize the pseudorange solely as a means to obtain the local clock correction. Since microsecond accuracy is adequate for that purpose, only single-frequency L_1 pseudorange capability with limited resolution was provided by NGRS-1.

The single-frequency pseudorange measurement was upgraded in NGRS-1 (1980) by replacing the 10-ns time-interval counter with a 20-ps counter. This improved the RMS noise level from 1.5 m (truncation limited) to 70 cm (receiver limited). NGRS-2, which utilizes the model 5010 receiver, has two 200-ps counters. In all cases, the observation is the time interval between the local 6-s epoch and the received epoch.

In order to obtain ionospheric corrected range difference observations, dual-frequency analog Doppler signals are used. Since these signals are analog, a counter external to the receiver is required. A 60-s nominal count interval was chosen. This method of providing continuous Doppler observations is used in both systems. At each local minute epoch, the current reading of the L_1 or L_2 Doppler counter is strobed and the time interval to the next positive zero crossing is measured. These two quantities are used to construct the cycle count during the previous 1-min interval. The range difference can then be computed using the two frequency observations[1].

The time-of-arrival difference for signals emanating from a satellite and received at two stationary (in the earth fixed frame) sites can be used to determine the baseline connecting the two sites. The data class described is a range difference in space at a common time. The NGRS are primarily designed to obtain range differences in time at a fixed site; consequently, the Doppler count data cannot be used directly in the time-of-arrival difference problem. If the two sites are considered to be independent and do not communicate in real time, the most straightforward arrangement with the NGRS is to plan the observations so that the two receivers track the same satellites simultaneously and record pseudoranges and Doppler counts in the usual manner. When the data are later processed, the pseudoranges from each satellite-to-site combination can be computed, evaluated at a common time, and differenced to obtain the desired range difference between the sites. Both the pseudorange and Doppler data are processed together. However, since the Doppler carries no absolute range information, the evaluation of the smoothed range is determined primarily by the quality of the pseudorange obsevations. The single-frequency measurements are adequate for relative positioning if the sites are not far apart, since then both receivers will see substantially the same ionospheric and tropospheric refraction effects.

FORMULATION

The first adjustment that must be made to the two data sets is to convert to a common time system. In this application, the broadcast ephemeris, the broadcast satellite clock corrections, and

the observed pseudoranges can be used to determine a set of polynomial coefficients that will convert local time to GPS time[2].

The 6-s pseudoranges are too frequent and too noisy to be used individually, so a smoothing polynomial is employed that also incorporates the range difference data. Only L_1 data are used, because NGRS-1 lacks L_2 pseudorange and the baseline involved is very short. The ionospheric correction to the L_1 range difference (derived from the Doppler) is computed and applied twice to account for the difference in sign between phase (Doppler) and group (range) delays introduced by the ionosphere[3]. The time tags attached to the pseudoranges are the local times of reception of the satellite epoch, while the range differences are tagged at the local epoch. These differ by the amount of the pseudorange measurement.

The smoothing range polynomial is defined as follows:

$$r(t_k) = a_o + \sum_{i=1}^{4} a_i (t_k - t_o)^i \tag{1}$$

In the case of range difference, it is $r(t_j) - r(t_{j-1})$.

$$r(t_j) - r(t_{j-1}) = \sum_{i=1}^{4} a_i [(t_j - t_o)^i - (t_{j-1} - t_o)^i] \tag{2}$$

These two observation equations are used together in one least squares solution to solve for the a_i's. In a typical 10-min fit, there are 100 pseudorange observations and 10 range difference observations. However, the range differences are more accurate and are weighted by a factor of 20 to 1 over the pseudoranges.

Similar 10-min data spans from each site are smoothed and the resulting coefficients are used in Equation 1 to compute a range at a time near the middle of the span. The ranges are then differenced to obtain the equivalent time-of-arrival difference of the satellite signal at the two sites. Instead of fitting first and then differencing, the data might have been differenced first and then fitted. This has the following advantages: allows the use of a lower-order polynomial, introduces less numerical error, and utilizes a single fit rather than two fits. However, because the local clocks were not necessarily synchronized, the data were not obtained simultaneously; consequently, this option was abandoned.

The geometry of the relative positioning problem is illustrated in Figure 1. The pertinent vectors are defined below.

t_T	time of transmission
t_R	time of reception
$\bar{r}_s(t_T) = x_s \hat{x} + y_s \hat{y} + z_s \hat{z}$	satellite position
$\bar{r}_g(t_R) = x_g \hat{x} + y_g \hat{y} + z_g \hat{z}$	reference site position
$\bar{r}_h(t_R) = x_h \hat{x} + y_h \hat{y} + z_h \hat{z}$	secondary site position
$\bar{b}(t_R) = \bar{r}_h(t_R) - \bar{r}_g(t_R)$	baseline vector
$r = \lvert\bar{r}_s(t_T) - \bar{r}_g(t_R)\rvert$	slant range, reference site
$r + \ell = \lvert\bar{r}_s(t_T) - \bar{r}_h(t_R)\rvert$	slant range, secondary site

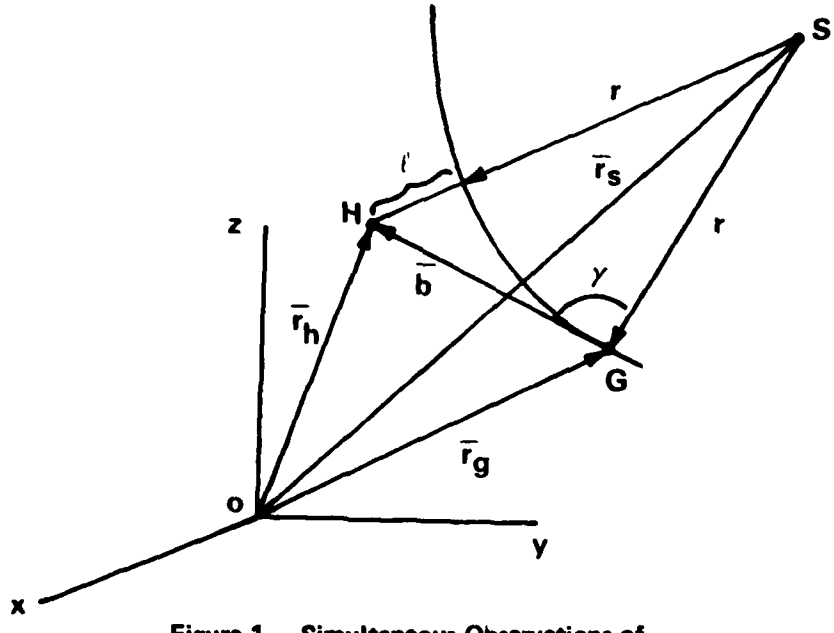

Figure 1. Simultaneous Observations of a Satellite From Two Sites

The x, y, z coordinate system in Figure 1 is an earth fixed frame; therefore, the vectors $\bar{r}_g$, $\bar{r}_h$, and $\bar{b}$ are independent of time. The satellite vector $\bar{r}_s(t_T)$ is the only time-variable parameter. The differences in range from the satellite to the two sites is represented by ℓ and is part of the observation obtained from differencing the two smoothing polynomials. The remaining portion of the observation is due to differences in receiver biases and will be represented by $\ell_1 + \ell_2(t_R - t_o)$. Thus, the observation equation is

$$L(t_R) = \ell + \ell_1 + \ell_2(t_R - t_o) \tag{3}$$

The geometric part, ℓ, is a function of the unknown baseline vector $\bar{b}$. In the triangle GHS,

$$(r + \ell)^2 = r^2 + b^2 - 2rb\cos\gamma \tag{4}$$

The term $rb\cos\gamma$ is the dot product $\bar{b} \cdot (\bar{r}_s - \bar{r}_g)$.

$$rb\cos\gamma = \bar{b} \cdot (\bar{r}_s - \bar{r}_g) = x_b(x_s - x_g) + y_b(y_s - y_g) + z_b(z_s - z_g) \tag{5}$$

Equation 4 can now be solved for ℓ by taking the square root and substituting Equation 5.

$$\ell = [r^2 + b^2 - 2\bar{b} \cdot (\bar{r}_s - \bar{r}_g)]^{1/2} - r \tag{6}$$

The parameters that are to be included in the solution are

$$x_b, y_b, z_b, \ell_1, \text{and } \ell_2,$$

which represent the baseline vector and the receiver differences.

For each parameter, there is an initial estimate that is to be improved by using the observations. The computed value L_c is obtained from Equation 3, using the initial estimates. The observed value is L_o. These will differ by an amount ΔL such that

$$L_o = L_c + \Delta L$$

The problem is linearized if L_c and ΔL are taken to be the first and second terms of a Taylor's series expanded about the initial estimate. The third and higher terms are omitted. The expanded second term is

$$\Delta L = \frac{\partial L_c}{\partial x_b}\Delta x_b + \frac{\partial L_c}{\partial y_b}\Delta y_b + \frac{\partial L_c}{\partial z_b}\Delta z_b + \frac{\partial L_c}{\partial \ell_1}\Delta \ell_1 + \frac{\partial L_c}{\partial \ell_2}\Delta \ell_2 \tag{8}$$

The required partial derivatives are obtained from Equations 3 and 6:

$$\frac{\partial L_c}{\partial x_b} = [r^2 + b^2 - 2\bar{b} \cdot (\bar{r}_s - \bar{r}_g)]^{-\frac{1}{2}} (x_b - x_s + x_g)$$

$$\frac{\partial L_c}{\partial y_b} = [r^2 + b^2 - 2\bar{b} \cdot (\bar{r}_s - \bar{r}_g)]^{-\frac{1}{2}} (y_b - y_s + y_g) \qquad (9)$$

$$\frac{\partial L_c}{\partial z_b} = [r^2 + b^2 - 2\bar{b} \cdot (\bar{r}_s - \bar{r}_g)]^{-\frac{1}{2}} (z_b - z_s + z_g)$$

$$\frac{\partial L_c}{\partial \ell_1} = 1$$

$$\frac{\partial L_c}{\partial \ell_2} = t_R - t_o$$

The system of equations represented by Equation 7 can be placed into matrix form and solved using weighted batch least squares. Each row represents one smoothed observation.

$$\begin{vmatrix} (L_o - L_c)_1 \\ (L_o - L_c)_2 \\ \vdots \\ (L_o - L_c)_n \end{vmatrix} = \begin{vmatrix} \left(\frac{\partial L_c}{\partial x_b}\right)_1 & \left(\frac{\partial L_c}{\partial y_b}\right)_1 & \left(\frac{\partial L_c}{\partial z_b}\right)_1 & 1 & (t_{R1} - t_o) \\ \left(\frac{\partial L_c}{\partial x_b}\right)_2 & \left(\frac{\partial L_c}{\partial y_b}\right)_2 & \left(\frac{\partial L_c}{\partial z_b}\right)_2 & 1 & (t_{R2} - t_o) \\ \vdots & \vdots & \vdots & \vdots & \vdots \\ \left(\frac{\partial L_c}{\partial x_b}\right)_n & \left(\frac{\partial L_c}{\partial y_b}\right)_n & \left(\frac{\partial L_c}{\partial z_b}\right)_n & 1 & (t_{Rn} - t_o) \end{vmatrix} \cdot \begin{vmatrix} \Delta x_b \\ \Delta y_b \\ \Delta z_b \\ \Delta \ell_1 \\ \Delta \ell_2 \end{vmatrix} \qquad (10)$$

The matrix of partials is denoted by A, and the parameters to be improved are denoted by X. The above then reduces to the form

$$L_o - L_c = AX$$

Then,

$$A^T WAX = A^T W (L_o - L_c)$$

and

$$X = (A^T WA)^{-1} A^T W (L_o - L_c)$$

The matrix $(A^T WA)^{-1}$ is the covariance matrix.

The diagonal weight matrix W is introduced to give smoothed observations with low noise more weight in the solution than those with high noise. The relative weights are obtained from the RSS of the RMS computed from the two smoothing polynomials that comprise the particular observation.

The solution vector X is then added to the initial estimate of

$$x_b, y_b, z_b, \ell_1, \text{and } \ell_2$$

to obtain the improved values. The standard deviation in this result is obtained from the square root of the diagonals of the covariance matrix. The confidence that one places in these standard deviations depends upon how well the fluctuations in the observations agree with the statistical assumptions inherent in the least-squares process. Unmodeled effects (e.g., systematic errors in $\bar{r}_s$ or variable instrumental biases) can lead to solutions whose true error is much larger than the computed standard deviation. When unmodeled effects are known to be present in the data, the standard deviations can only be viewed as a guide indicating the geometric strength of the observations and subsequent solution.

OBSERVATIONS

January 1981, both NGRS-1 and NGRS-2 were operated side by side at NSWC. Pseudorange and Doppler data were recorded in the usual manner while the receivers simulaneously observed the same GPS satellites. Two antenna sites were in use: a surveyed site and a site approximately 2 m south. The receivers spent time connected to a common antenna and to their individual antenna. Also, a common frequency standard was used, as well as individual frequency standards. Table 2 lists the number of 20-min segments obtained from each satellite on each day. For each segment, a residual difference in range is computed.. The mean and standard deviations of these residuals for all segments on a given day are presented. The significance of these residuals is discussed in the next section.

Table 2. Segment Statistics For Each Days Observations

Day (January 1981)	10	12	15	16	17	18	19
Antenna	Common		Separate		Common		
Frequency Standard	Common		Common		Separate		
SV-5							
Number of Segments	23	32	25	22	27	28	14
Mean (m)	0.129	0.138	0.207	0.208	0.112	0.116	0.107
Standard Deviation (m)	0.019	0.026	0.038	0.032	0.021	0.024	0.014
SV-6							
Number of Segments	14	8	11	14	14	14	13
Mean (m)	0.110	0.114	0.218	0.221	0.086	0.091	0.095
Standard Deviation (m)	0.009	0.018	0.025	0.042	0.018	0.011	0.015
SV-8							
Number of Segments	10	0	8	12	15	15	16
Mean (m)	0.109		0.188	0.220	0.090	0.090	0.094
Standard Deviation (m)	0.013		0.007	0.025	0.024	0.019	0.012
SV-9							
Number of Segments	18	18	17	7	18	16	5
Mean (m)	0.158	0.154	0.212	0.265	0.133	0.144	0.149
Standard Deviation (m)	0.038	0.032	0.025	0.062	0.031	0.027	0.031

NOISE PROBLEM

Unfortunately, a problem with the 5010 receiver in NGRS-2 caused the pseudorange observations to have a higher noise level than comparable observations obtained from NGRS-1. This fault, which was later identified and corrected, degraded the NGRS-2 pseudorange data somewhat. The nature of the degradation is illustrated by the Figures 2 through 5.

Twenty-min segments of data were fit by a fourth-degree polynomial, as previously described. Both L_1 6-s pseudoranges and L_1 60-s integrated Doppler range differences contributed to the fit. Figure 2 shows plots of the fit residuals of two consecutive 20-min segments of data from NGRS-1. Figure 3 shows similar residuals over the same span from NGRS-2. The diamond symbols represent range difference residuals from Doppler, added consecutively to produce a biased range. For plotting purposes, the bias was supplied by evaluating the polynomial at the time of the beginning

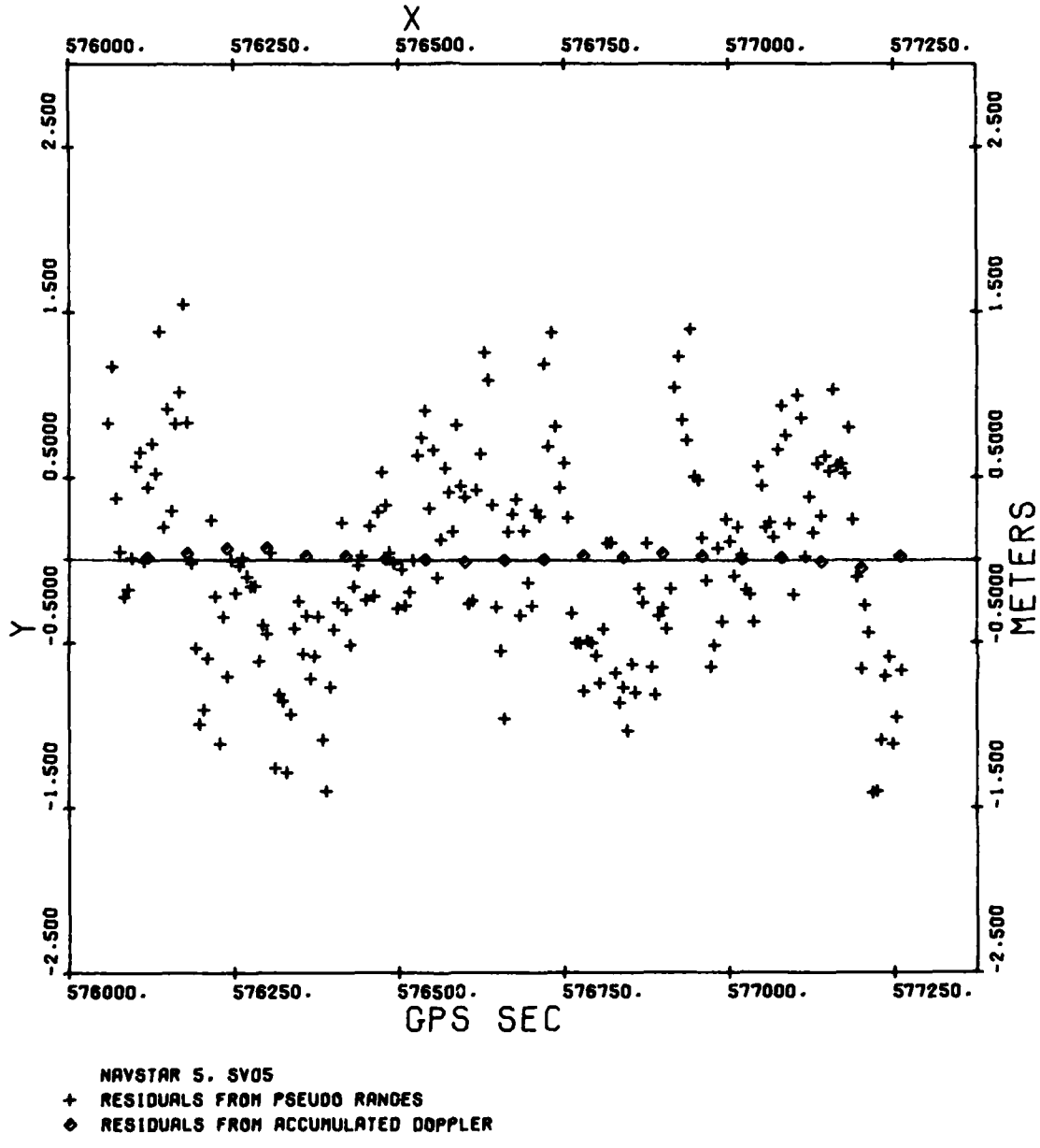

(a)

Figure 2. NGRS-1 Residuals From 20-Min Smoothing Polynomial, NSWC/Dahlgren, Day 10, 1981

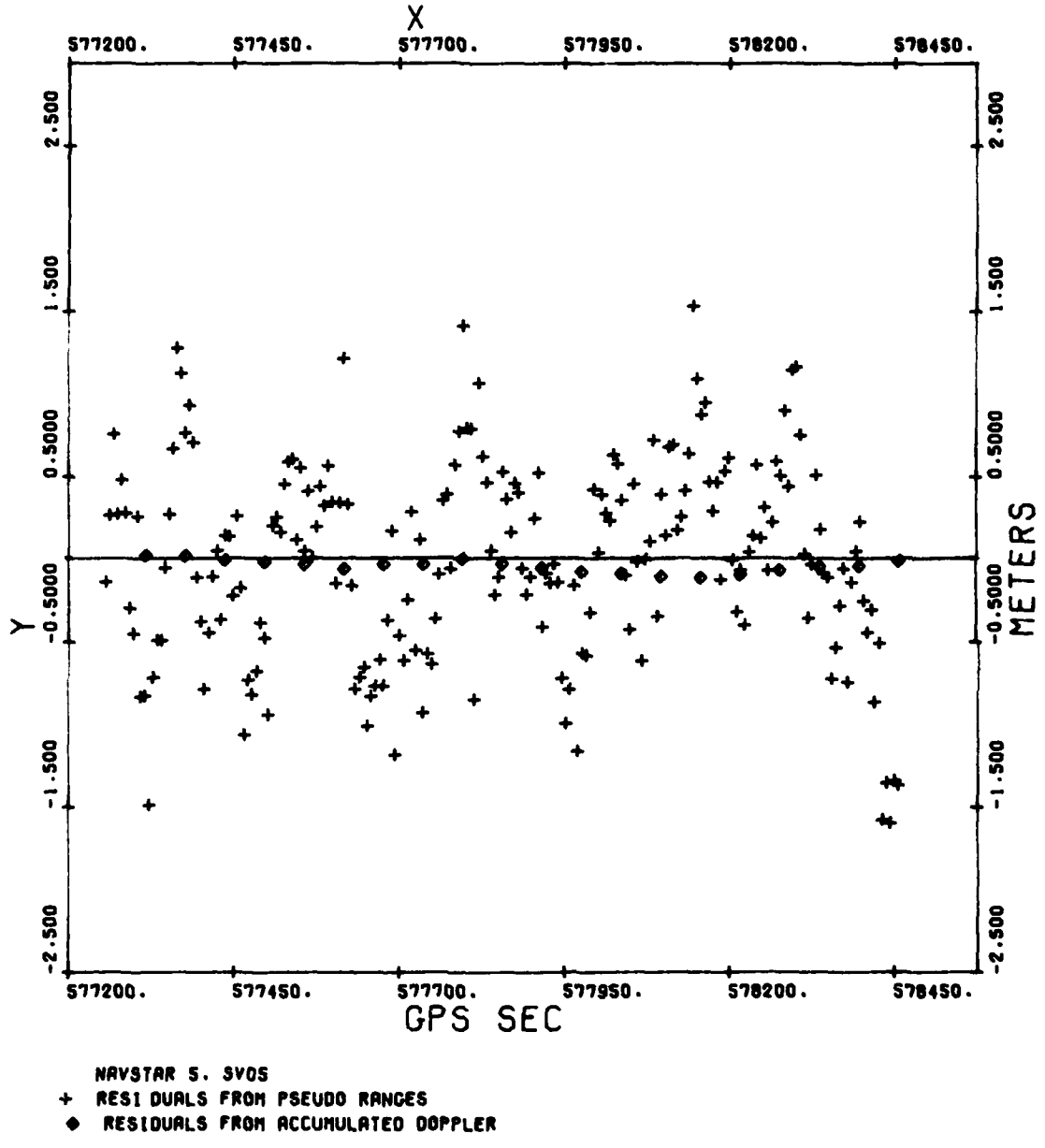

(b)

Figure 2. NGRS-1 Residuals From 20-Min Smoothing Polynomial, NSWC/Dahlgren, Day 10, 1981 (Continued)

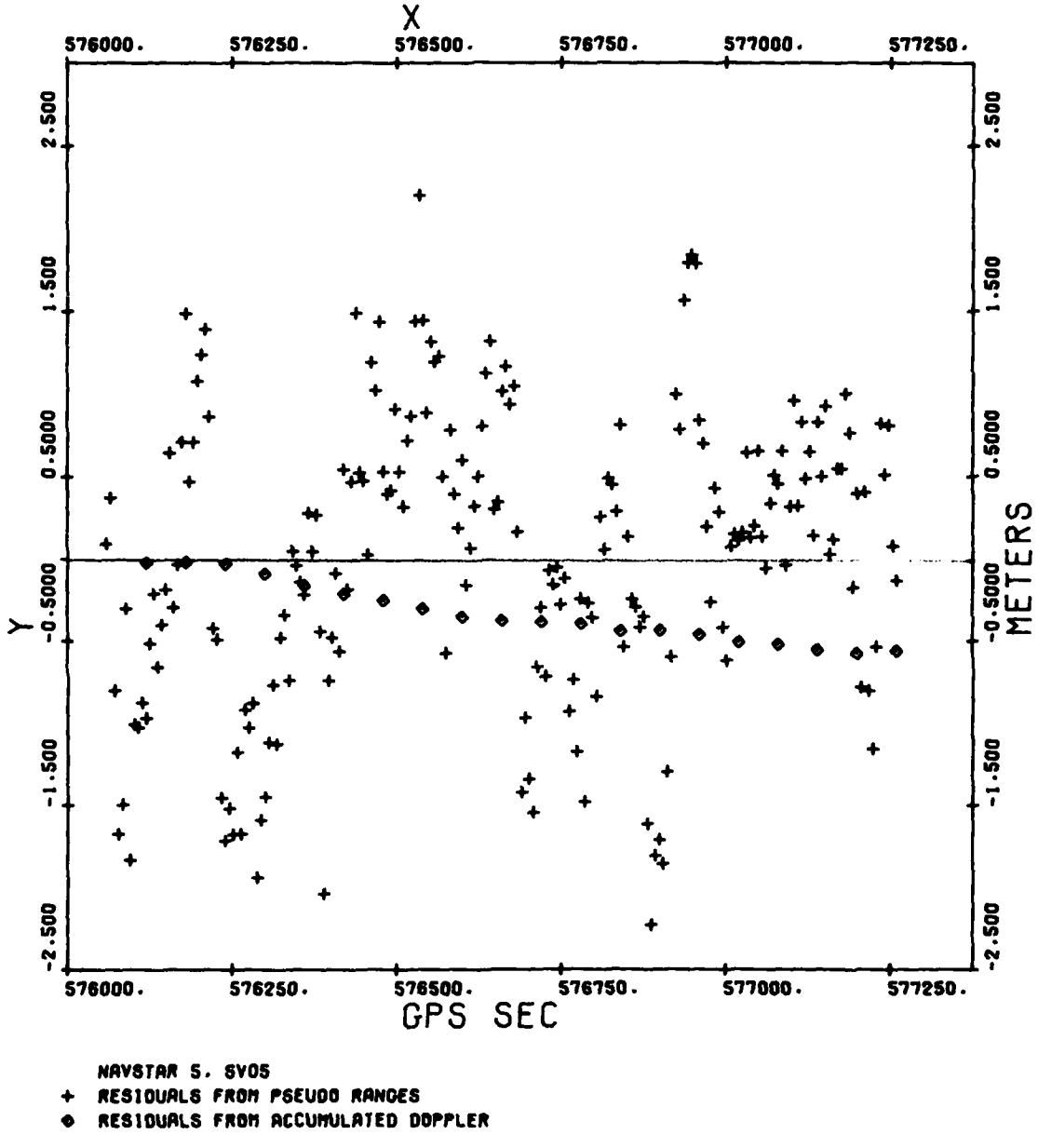

(a)

Figure 3. NGRS-2 Residuals From 20-Min Smoothing Polynomial, NSWC/Dahlgren, Day 10, 1981

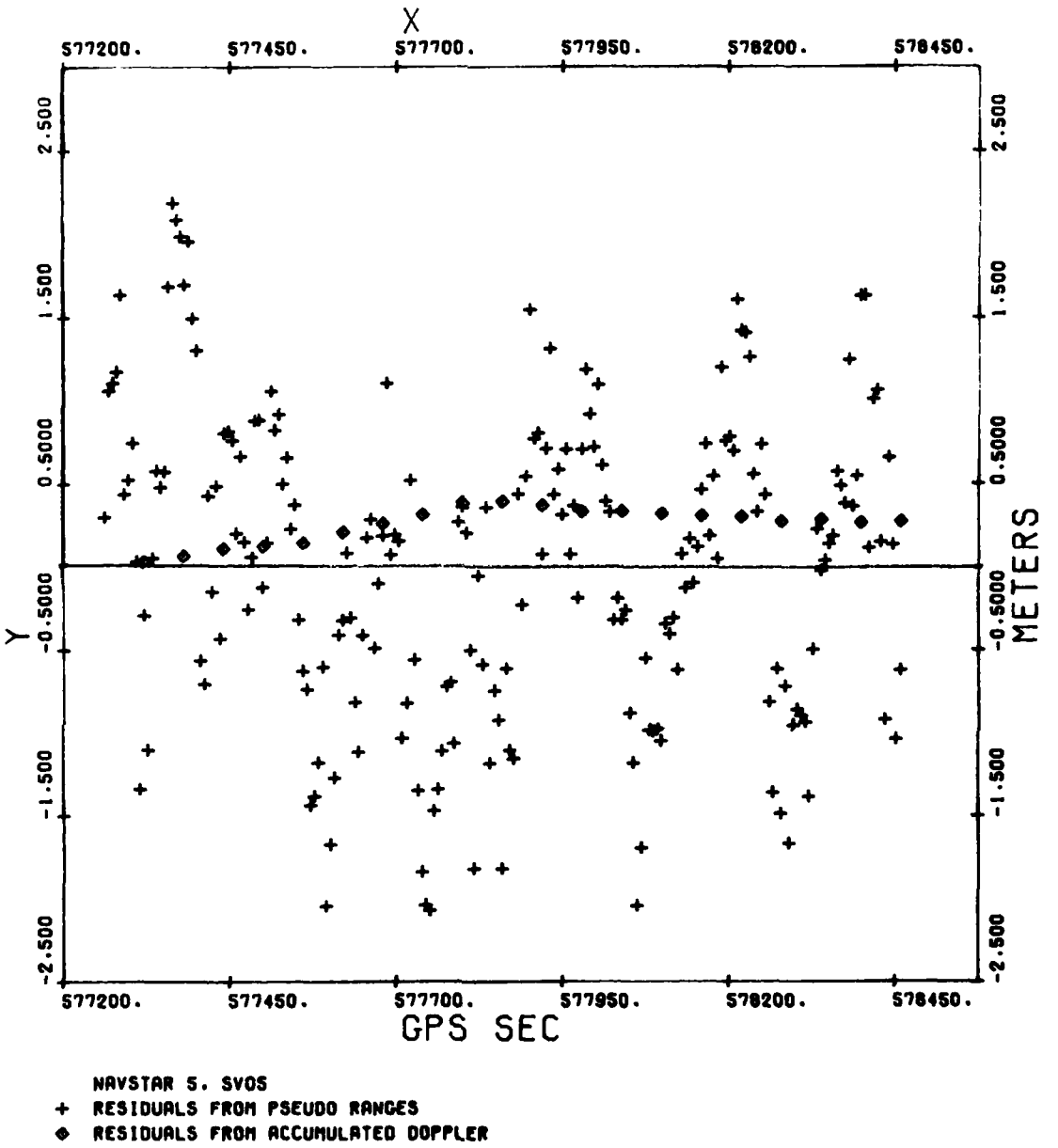

(b)

Figure 3. NGRS-2 Residuals From 20-Min Smoothing Polynomial, NSWC/Dahlgren, Day 10, 1981 (Continued)

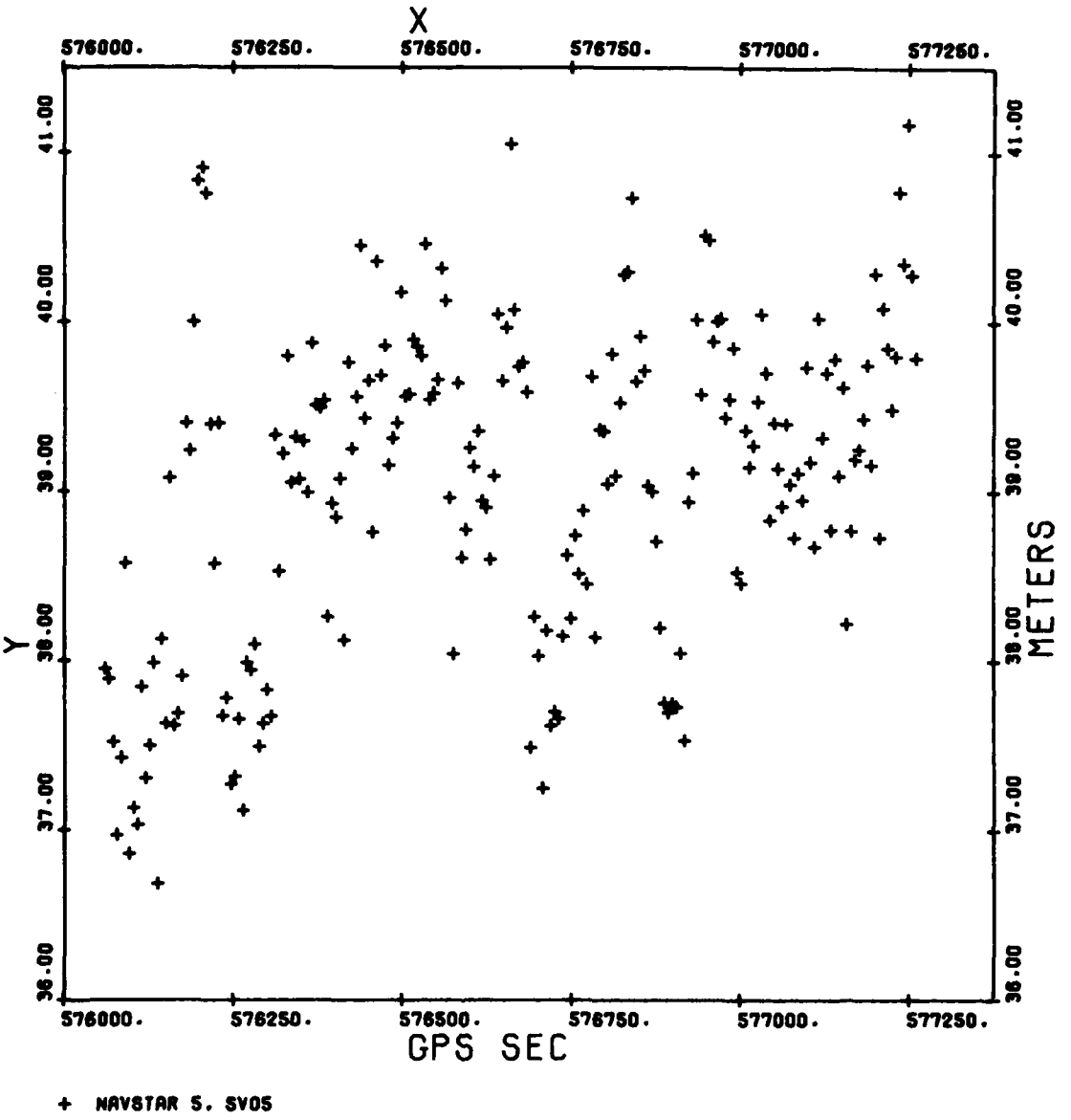

(a)

Figure 4. Differences in Pseudorange (20-Min), NGRS-2-NGRS-1, NSWC/Dahlgren, Day 10, 1981

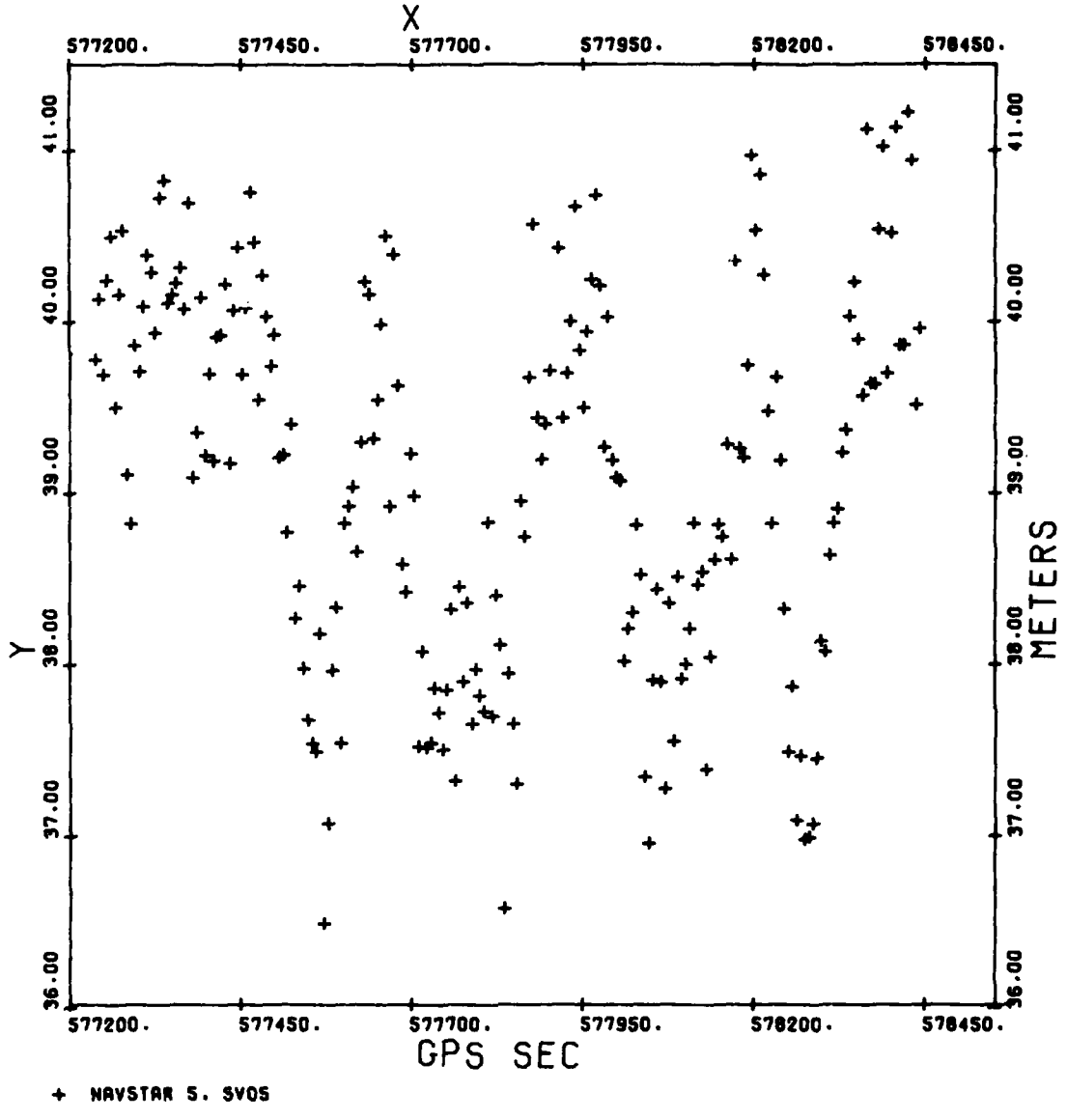

(b)

Figure 4. Differences in Pseudorange (20-Min), NGRS-2-NGRS-1, NSWC/Dahlgren, Day 10, 1981 (Continued)

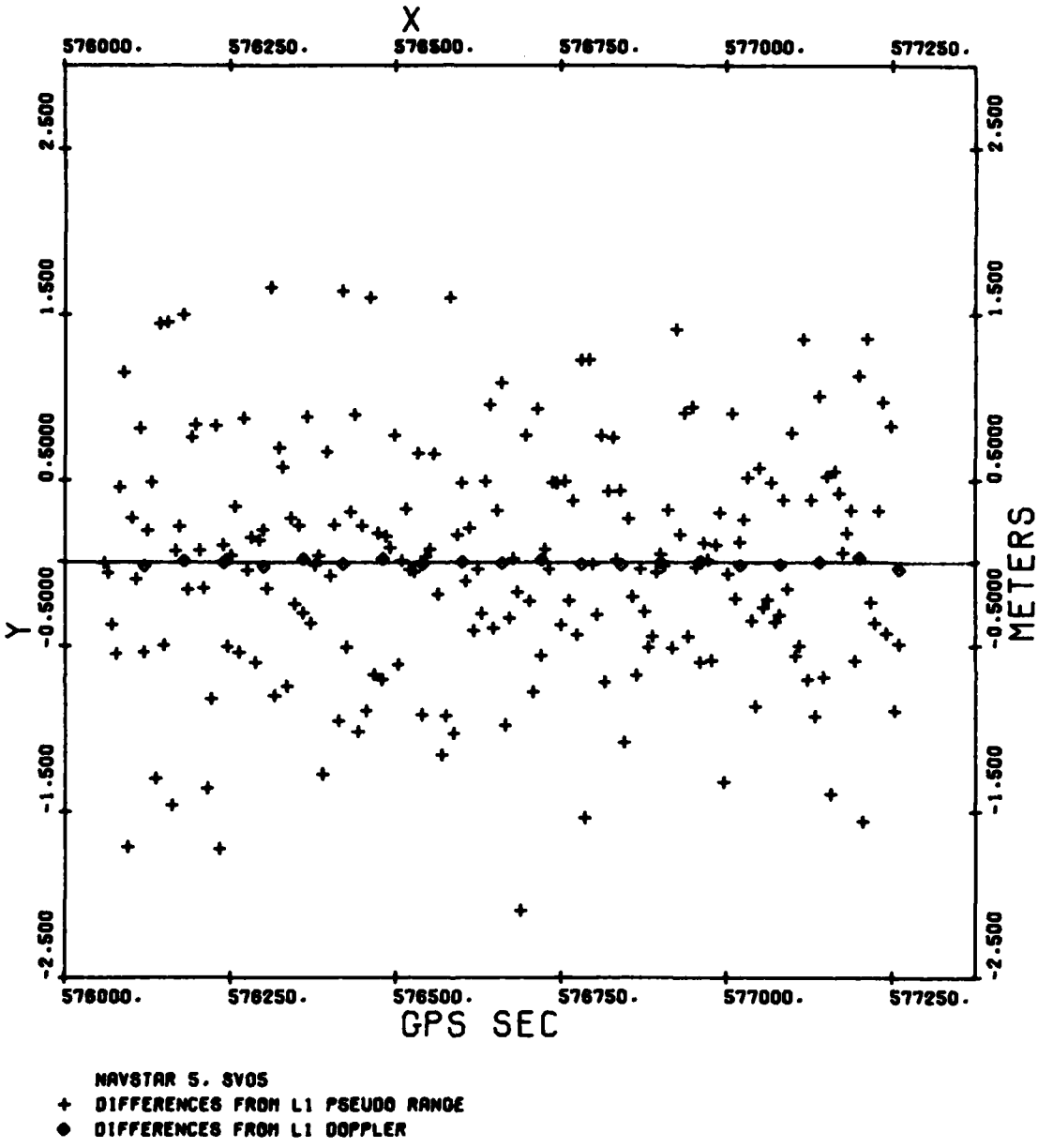

(a)

Figure 5. Differences in Range Differences, NGRS-2-NGRS-1, NSWC/Dahlgren, Day 10, 1981

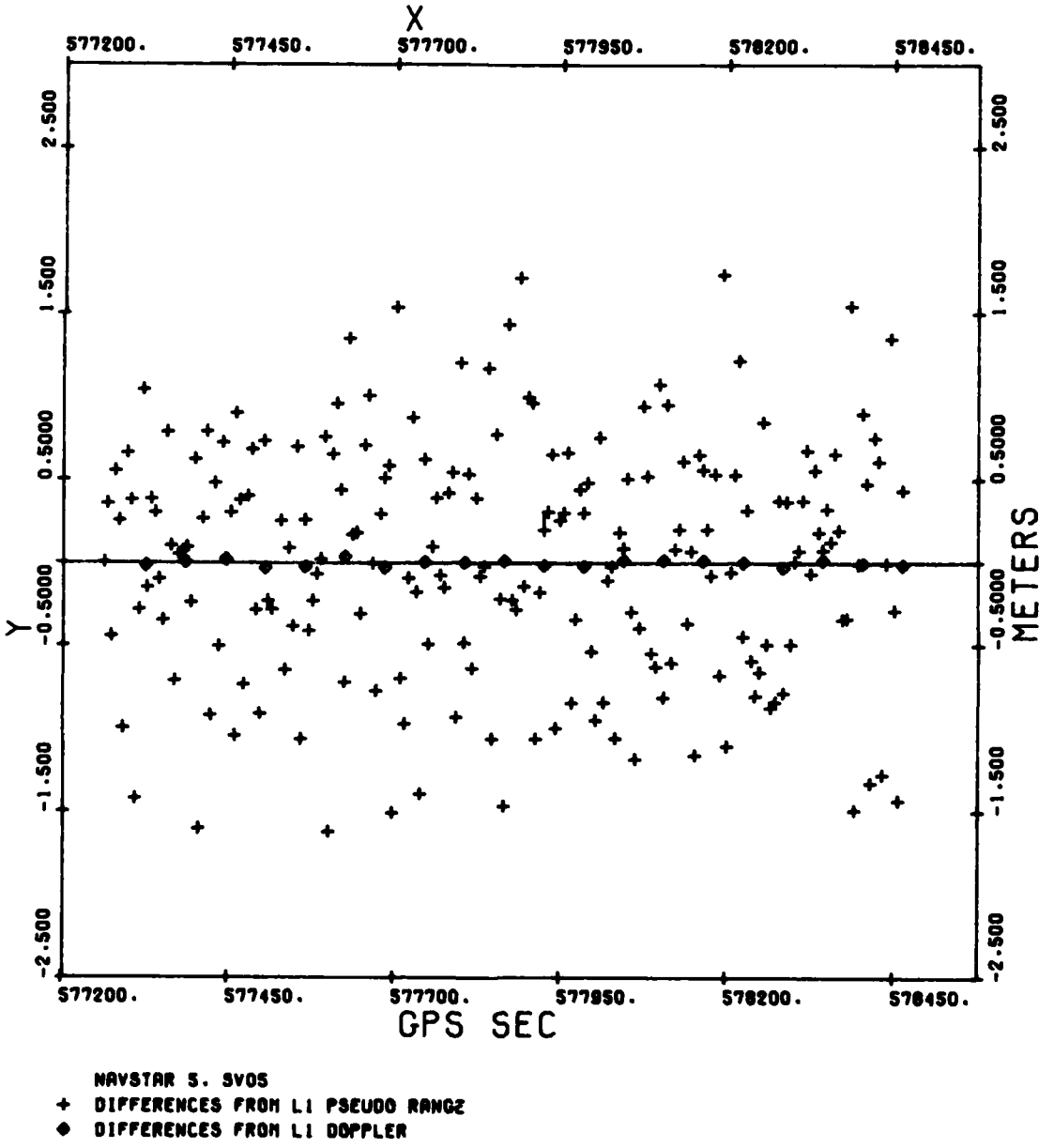

(b)

Figure 5. Differences in Range Differences, NGRS-2-NGRS-1, NSWC/Dahlgren, Day 10, 1981 (Continued)

of the first Doppler observation. The plus symbols are the pseudorange residuals. In the case of NGRS-1, the biased ranges and pseudorange are consistent, since the residuals are centered about zero. In the case of NGRS-2, the consistency is not as good.

In Figure 3(a) the biased range residuals deviate below the zero axis; and in Figure 3(b), they deviate above the axis. The problem appears to be a random short-term drift in the NGRS-2 pseudoranges. Evidence for this has been gathered by plotting the differences of the pseudoranges obtained from the two receivers. The differences should be constant over the interval, because both receivers were connected to the same antenna and both were being driven by the same frequency standard. The difference plots (Figures 4) show several meters of scatter and a tilt with positive slope (Figure 4a) and negative slope (Figure 4b). The differences in range differences between the two receivers (Figure 5) show no similar trends; thus, the fault appears to lie with the pseudorange bias from NGRS-2. The computed RMS for all these residual plots is listed in Table 3.

Table 3. RMS of Residual Plots

	Figure	NGRS	SPAN	RMS (m)
Smoothing Polynomial	2a	1	1	0.59
	2b	1	2	0.57
	3a	2	1	0.85
	3b	2	2	0.88
Pseudorange Differences	4a	2-1	1	0.95
	4b	2-1	2	1.09
Differences of Range Differences	5a	2-1	1	0.68
	5b	2-1	2	0.68

SOLUTIONS

DAYS 10 AND 12

Data from the two days in which the receivers used common antennas and common frequency standards have been processed in the manner described in the previous sections. Figure 6 shows the segments of the satellite ground tracks observed on day 10. The tracks for day 12 were similar, except that the observations of SV-8 were omitted.

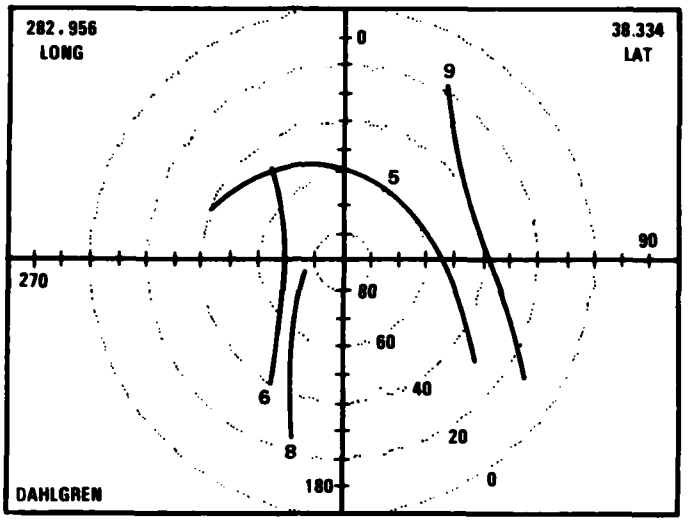

Figure 6. Azimuth and Elevation Tracks of Satellites From Site on Day 10

All observations were smoothed over a period of 10 min; therefore, they consist of 100 pseudoranges and 10 range differences. The number of 10-min segments available on each day is listed in Table 2. The baseline vector $\bar{b}$ was purposely offset by 4 m in each-earth fixed component in these solutions in order to demonstrate that the data produces corrections to $\bar{b}$ in the correct direction. These corrections should be -4 m in each component. The results obtained are summarized in Table 4. A second solution was performed in which the parameter ℓ_2 was constrained, by a priori sigmas, to zero. This procedure improved the result on day 10, but worsened the result on day 12. Table 5 presents this solution.

An additional experiment using just six 10-min segments was performed. These segments (Table 6) were selected so that they were spread in azimuth around the site and were nearly the same on day 12 as on day 10. Observations from SV-8 were omitted from both. The solutions obtained are quite reasonable (Table 7) and illustrate the importance of choosing observations that cover the site from all sides. Similar solutions using data from just one satellite (SV-6, SV-8, or SV-9) were poor due to the absence of data from two or more quadrants.

DAYS 15 AND 16

Data from the two days in which the receivers used common frequency standards but separate antennas were processed; the baseline was to be assumed zero. In fact, the antenna for NGRS-2 was placed 2 m south and 0.2 m east of the NGRS-1 antenna. On day 15, the satellites observed were SV-5, 6, and 9; on day 16, SV-5, 6, and 8 were observed. A solution using these data is presented in Table 8. Separate solutions using only the data from each day are given in Table 9. All of these solutions are rotated from earth-fixed components to a local vertical frame with components that are labeled North, East, and Vertical, so that comparison with the known baseline is possible.

Even though the standard deviations indicate that the vertical component is the best-determined of the three components, it contributes the largest error. The excessive receiver noise during these two days (as noted in Table 2) may have been a contributing factor to the poor results obtained in this component.

DAYS 17, 18, AND 19

During the last three days of this experiment, the two systems operated from independent frequency standards, but utilized a common antenna. The solutions obtained were comparable with those on days 10 and 12, when a common frequency standard was used. The values for the bias ℓ_1 and drift ℓ_2 are larger than they had previously been because of the addition of the relative epoch offset that exists between the two frequency standards.

A combined solution using all the data collected during these three days (a total of 195 10-min segments) is presented in Table 10. Again, a 4-m offset in each component was introduced. Separate solutions for days 18 and 19 were also made (Table 11). Though the standard deviations are smaller in the three-day solution, the magnitude of the error is greater than that found in the single-day solutions. This result tends to indicate that the bias model fits the data better over a short time span. A result similar to this has been predicted by Fell[4].

Table 4. Solutions Using All Available Data, Days 10 and 12

Day	Component	Solution	Sigma	Solution - True	Units
10	x	-3.570	0.052	0.430	m
	y	-5.171	0.109	-1.171	m
	z	-3.448	0.090	0.552	m
	ℓ_1	38.580	0.093	–	m
	ℓ_2	17.658×10^{-6}	0.996×10^{-6}	–	m/s
12	x	-3.955	0.060	0.045	m
	y	-4.432	0.130	-0.432	m
	z	-3.830	0.101	0.170	m
	ℓ_1	38.499	0.105	–	m
	ℓ_2	-1.714×10^{-6}	0.935×10^{-6}	–	m/s

	Day 10	Day 12
Magnitude (Solution - True)	1.364	0.466

Table 5. Solutions Using All Available Data, Parameter ℓ_2 Constrained, Days 10 and 12

Day	Component	Solution	Sigma	Solution - True	Units
10	x	-3.543	0.052	0.457	m
	y	-4.181	0.094	-0.181	m
	z	-4.279	0.076	-0.279	m
	ℓ_1	38.419	0.093	–	m
	ℓ_2	0.0	0.0	–	m
12	x	-3.978	0.059	0.022	m
	y	-4.555	0.112	-0.555	m
	z	-3.719	0.080	0.281	m
	ℓ_1	38.540	0.103	–	m
	ℓ_2	0.0	0.0	–	

	Day 10	Day 12
Magnitude (Solution - True)	0.565	0.622

Table 6. Azimuth And Elevation of Six Segments Selected From Days 10 and 12

	Azimuth (Degrees)		Elevation (Degrees)	
	Day 10	Day 12	Day 10	Day 12
SV-5	310.8	313.5	46.2	47.0
	116.9	115.9	40.1	40.8
SV-6	230.4	226.5	61.6	59.4
	211.5	210.6	42.6	41.0
SV-9	85.4	85.4	39.0	39.1
	33.9	33.9	21.9	21.9

Table 7. Solutions Using Six Selected Segments, Days 10 and 12

Day	Component	Solution	Sigma	Solution - True	Units
10	x	-3.805	0.197	-0.195	m
	y	-3.768	0.380	-0.232	m
	z	-4.552	0.376	0.552	m
	ℓ_1	37.356	0.361	–	m
	ℓ_2	18.736×10^{-6}	3.426×10^{-6}	–	m/s
12	x	-3.557	0.622	-0.443	m
	y	-5.052	0.373	1.052	m
	z	-3.192	0.414	-0.808	m
	ℓ_1	39.264	0.557	–	m
	ℓ_2	-5.178×10^{-6}	10.559×10^{-6}	–	m/s

	Day 10	Day 12
Magnitude (Solution - True)	0.630	1.399

Table 8. Combined Solution Using All Available Data, Days 15 and 16

Day	Component	Solution	Sigma	Solution - True	Units
15	North	-2.122	0.157	-.122	m
and 16	East	0.553	0.100	.353	m
	Vertical	-1.353	0.035	-1.653	m
	ℓ_1	49.276	0.133	–	m
	ℓ_2	-1.104×10^{-6}	0.557×10^{-6}	–	m/s

	Days 15 and 16
Magnitude (Solution - True)	1.695

Table 9. Separate Solutions, Days 15 and 16

Day	Component	Solution*	Sigma	Solution - True	Units
15	North	-2.672	0.507	-.672	m
	East	-0.018	0.233	-.220	m
	Vertical	1.200	0.232	1.200	m
	ℓ_1	50.228	0.185	–	m
	ℓ_2	-38.980×10^{-6}	12.878×10^{-6}	–	m/s
16	North	-1.844	0.307	0.156	m
	East	0.869	0.178	0.669	m
	Vertical	-3.727	0.104	-3.727	m
	ℓ_1	47.254	0.538	–	m
	ℓ_2	0.366×10^{-6}	6.396×10^{-6}	–	m/s

	Day 15	Day 16
Magnitude (Solution - True)	1.393 m	3.790 m

*Day 15: SV-5, 6, 9
Day 16: SV-5, 6, 8

Table 10. Combined Solution Using All Available Data, Days 17, 18, and 19

Day	Component	Solution	Sigma	Solution - True	Units
17, 18, and 19	x	-4.512	0.030	-0.512	m
	y	-5.548	0.047	-1.548	m
	z	-3.327	0.032	0.673	m
	ℓ_1	-3177.808	0.046	–	m
	ℓ_2	-136.653×10^{-6}	0.102×10^{-6}	–	m/s

	Days 17, 18 and 19
Magnitude (Solution - True)	1.764 m

Table 11. Separate Daily Solutions, Days 18 and 19

Day	Component	Solution	Sigma	Solution - True	Units
18	x	-4.869	0.052	-0.869	m
	y	-4.432	0.114	-0.432	m
	z	-4.029	0.057	-0.329	m
	ℓ_1	-3179.838	0.202	–	m
	ℓ_2	-118.217×10^{-6}	2.206×10^{-6}	–	m/s
19	x	-3.887	0.058	0.133	m
	y	-5.402	0.124	-1.402	m
	z	-3.762	0.062	0.238	m
	ℓ_1	-3184.151	0.408	–	m
	ℓ_2	-96.008×10^{-6}	2.334×10^{-6}	–	m/s

	Day 18	Day 19
Magnitude (Solution - True)	1.303 m	1.427 m

CONCLUSIONS

Relative positioning on a short baseline using single-frequency pseudoranges and range differences from Doppler is permissible if the mission accuracy requirements are set at 2-m or greater. The time on site need not be great if enough satellites are in view to satisfy the geometric requirements of the desired solution. This is demonstrated by the data in Table 6, for which only 1 hr (six 10-min segments) of observations were used to produce a solution with errors comparable to those obtained from 10 times as much data.

The standard deviations in all cases were highly optimistic when compared with the actual errors obtained. This indicates that the RMS of the residuals to each segment is not representative of the true errors involved. There appears to be something akin to time-variable channel biases operating that cannot be absorbed by the ℓ_1 and ℓ_2 parameters. Some method for on-line calibration, using locally generated stable test signals, is needed in order to derive corrections for this interchannel bias fluctuation.

Other methods of treating these data are capable of producing better results. In particular, relative positioning using the Doppler data alone allows a more precise solution to be obtained. Figures 2 and 3 can be used to indicate the superior quality of the accumulated Doppler vs the pseudoranges for this data set. Processing of this same data span using Doppler only has been reported elsewhere.[5]

REFERENCES

1. B. R. Hermann, ***Formulation for the NAVSTAR Geodetic Receiver System (NGRS)***, NSWC TR 80-348 (Dahlgren, Va., March 1981).

2. B. R. Hermann, ***Time Correction of Data From the NAVSTAR Geodetic Receiver System (NGRS)***, NSWC TR 81-174 (Dahlgren, Va., August 1981).

3. P. S. Jorgensen, ***Ionospheric Measurements From NAVSTAR Satellites***, The Aerospace Corporation (El Segundo, Calif., July 1979).

4. P. J. Fell, ***Geodetic Positioning Using A Global Positioning System of Satellites***, Department of Geodetic Science Report NO. 299 (Ohio State University, June 1980).

5. B. R. Hermann and A. G. Evans, ***A Demonstration of Relative Positioning Using Conventional GPS Doppler Receivers***, IEEE National Telecommunications Conference Proceedings, New Orleans, La. (November 1981).

DISTRIBUTION

Shell Resources Canada Ltd.
400 4th Ave. S.W.
ATTN: Alex Hittel (4)
Calgary, Alberta
Canada T2P0J4

TASC
6 Jacob Way
ATTN: Gary Matchett
Reading, MA 01867

Charles R. Payne
6592/SPO, Code YED
P.O. Box 92960
World Way Postal Center
Los Angles, CA 90009

AFGL - PHP
Hanscom AFB
ATTN: Jack Klobuchar
Bedford, MA 01731

STI
1195 Bordeaux Drive
ATTN; J. J. Spiker, Jr. (5)
Sunnyvale, CA 94086

IBM
18100 Frederick Pike
ATTN: Fritz Byrne (3)
Gaithersburg, MD 20760

Applied Physics Laboratory
Johns Hopkins University
Johns Hopkins Road
ATTN: Reginal Rhue
Joseph Wall
Edward Prozeller
Laurel, MD 20810

DISTRIBUTION (Continued)

Defense Mapping Agency Headquarters
U.S. Naval Observatory
Building 56
ATTN: Dr. Charles Martin (STT)
Washington, DC 20305

Defense Mapping Agency
Aerospace Center
2nd & Arsenal St.
ATTN: George Stentz (2)
St. Louis, MO 63118

Professor Charles Counselman III
54-620 Massachusetts Institute of Technology
77 Massachusetts Ave.
Cambridge, MA 02139

Dr. Peter Bender
Joint Institute for Laboratory Astrophysics
University of Colorado
Boulder, CO 80302

CAPT John Bossler
6001 Executive Blvd.
ATTN: 0A/C1X8
Rockville, Md 20852

Mr. Clyde Goad
6001 Executive Blvd.
ATTN: 0A/C1X8
Rockville, MD 20852

Defense Mapping Agency
Hydrographic/Topographic Center
Code GST
6500 Brookes Lane
ATTN: Ben Roth
Hand Heuerman
Fran Varnum
Caroline Leroy (3)
Washington, DC 20315

DISTRIBUTION (Continued)

U.S. Geological Survey
526 National Center
12201 Sunrise Valley Drive
ATTN: COL Paul E. Needham
Reston, VA 22092

University of Texas
Applied Research Laboratory
Post Office Box 8029
ATTN: Dr. Arnold Tucker
Dr. James Clynch
Austin, TX 78712

Naval Research Laboratory
Code 7966
Building 53
ATTN: James Buisson (2)
Washington, DC 20315

Transportation System Center
DST 542
Kendall Square
ATTN: John Kraemer
Cambridge, MA 02142

Magnavox Research Laboratory
2829 Moricopa St.
ATTN: Tom Stansel
Torrance, CA 90503

Defense Technical Information Center
Cameron Station
Alexandria, VA 22314 (12)

Library of Congress
ATTN: Gift and Exchange Division (4)
Washington, DC 20540

DISTRIBUTION (Continued)

Local:

E31 (GIDEP)	
E411 (Hall)	
F14 (Saffos)	(8)
K05	
K10	
K13 (Hermann)	(10)
K13 (Evans)	(10)
X210	(6)


DATE
ILME
8